Check for updates

Highly adhesive chitosan/poly(vinyl alcohol) hydrogels *via* the synergy of phytic acid and boric acid and their application as highly sensitive and widely linear strain sensors†

Cuiwen Liu, Ru Zhang, Yao Wang, Chengmeng Wei, Feng Li, Ning Qing and Liuyan Tang [ID] *

In recent years, flexible strain sensors have attracted increasing interest, and accurate sensing and comfortable wearables are highly demanded. However, current flexible strain sensors fail to have wide linearity and high sensitivity simultaneously, and their adhesion is insufficient for convenient wear and precise motion monitoring. Herein, chitosan/poly(vinyl alcohol) hydrogels with phytic acid (PA) and boric acid (BA) as crosslinkers (CS/PVA–PA–BA hydrogels) were fabricated. The synergy of phytic acid and boric acid not only improved the mechanical properties of the obtained hydrogels (1070% of fracture strain and 0.83 MPa of fracture stress), but also provided them with outstandingly strong adhesion. Their adhesive strength was up to 527 kPa for a variety of materials, including glass, silica rubber, steel, polytetrafluoroethylene (PTFE), and skin. In addition, the hydrogel-based strain sensor demonstrated high sensitivity (gauge factor = 4.61), a wide linear strain range (up to 1000%, R^2 = 0.996), fast response time (90 ms), and good stability. A flexible strain sensor with such high sensitivity and wide linear range simultaneously, to the best of our knowledge, has never been reported before. The development of CS/PVA–PA–BA hydrogels is expected to inspire a novel method for high-adhesive and high-sensing-performance wearable electronics.

New concepts

It was a challenge to develop highly sensitive strain sensors with a wide linear range owing to the trade-off between linearity and sensitivity. In this study, we design widely linear, and highly sensitive strain sensors made of chitosan/poly(vinyl alcohol) hydrogels. The strain sensor exhibited a sensitivity of 4.61 with a linear strain range of 1000%, which is the first strain sensor that has such high sensitivity and wide linear range simultaneously. The excellent sensing performance of the sensor was linked to the microstructure and conductive components of the prepared hydrogels. Additionally, this study utilized the synergy of phytic acid and boric acid to efficiently improve the adhesion of the hydrogels. While phytic acid provided the interface adhesion, boric acid improved the cohesion. Especially, their adhesive strength on pigskin reached 103 kPa, which was beyond that of many commercially available adhesives. This work breaks through the trade-off between sensitivity and linearity of strain sensors and highlights a strategy to fabricate highly adhesive hydrogels, paving the way to develop high-performance sensing materials for emerging electrical applications.

1. Introduction

Because of their inherent properties, such as flexibility, tunable mechanical properties, ionic or electrical conductivity, and biocompatibility, flexible strain sensors have potential applications in numerous fields, such as wearable devices,[1–4] soft robots,[5,6] and human–machine interfaces.[7,8] An ideal flexible strain sensor should demonstrate excellent sensing performance, including high sensitivity, a wide sensing range, a high

linear relationship, and good reproductivity.[9] The high sensitivity and wide sensing range are crucial to accurately detecting both small activities, such as speaking, heartbeat, and respiration, as well as large deformations, like joint and muscle movements.[10,11] The linear relationship between the applied strain and the relative resistance change of a sensor can simplify the calibration process in practical applications, improving the sensing precision and saving costs.[12] Although the sensitivity and strain sensing range of strain sensors have made great progress in recent years, their linearity is still poor.[13–15] In general, there is a trade-off between high sensitivity and wide linearity, since high sensitivity requires the microstructure of a hydrogel to change drastically even at small strains, whereas wide linearity needs a hydrogel to maintain its structural connection at high strains.[16] Therefore, developing a flexible sensor with high sensitivity and a wide linear relationship is still a challenge.

Due to their great ductility and inherent biocompatibility, conductive hydrogels are excellent candidates for the

School of Biotechnology and Health Sciences, Wuyi University, Jiangmen, 529020, China. E-mail: wyuchemtangly@126.com, tangly@wyu.edu.cn

fabrication of flexible strain sensors.[17] However, the abundance of water in hydrogel matrices creates a thin boundary layer, which prevents most hydrogel-based strain sensors from adhering to human skin directly. These sensors need to be fixed with adhesive tapes or bandages, which leads to uncomfortable wearing and inaccurate output signals.[18] To address this problem, previous studies generally improved the adhesion of hydrogel-based strain sensors by adding adhesive components such as dopamine,[19] nucleobase,[20] and protein.[21] Nevertheless, the costs of these components are generally high, with inadequate adhesive strength or sensing performance, which cannot satisfy industrial production.

Phytic acid (PA) is a common natural organic acid extracted from plant seeds, which is inexpensive, biocompatible, and biodegradable.[22] It has six phosphate groups, which can generate H^+ to provide hydrogels with conductivity.[23] These phosphate groups can also form hydrogen bonds with surfaces containing hydroxyl groups, or ionic bonds with surfaces containing cationic functional groups, and thus PA has also been used to fabricate adhesive hydrogels. For instance, Wang *et al.* prepared Janus hydrogel tapes using PA as the adhesive compound to form the adhesive layer and assembled this layer with a non-adhesive layer for strain sensors.[24] Yu *et al.* utilized PA as the adhesive compound to develop a novel polyvinylpyrrolidone/PA/MXenes hydrogel that had adhesion, injectability, self-healing property, and conductivity.[25] However, the adhesive strength of the reported hydrogels with PA is still not high enough to meet the practical requirement.

Boric acid (BA) is an electrophile that tends to bind to nucleophiles and various surfaces with abundant electron-donating groups (–OH, O, or N atoms). It is reported that the synergy of BA with other adhesive components could improve the adhesion of various materials.[26–28] For example, Efhamisisi *et al.* designed an adhesive using BA and tannin to increase the tensile shear strength and found that 4% of the tannin and BA content raised the shear strength to 53.55%.[29] This synergistic effect was also found by using the transglutaminase and BA derivatives to enhance the adhesion of soy protein adhesives.[30] The adhesive strength of the adhesives improved 138.5% due to the increase in cohesion and bond strength. Thus, it seems that the cooperation of PA and BA is a good strategy to improve the adhesive strength of hydrogels, but it has yet to be explored.

Herein, we develop a series of conductive hydrogels using PVA and chitosan (CS) to form hydrogel matrices and PA and BA as the crosslinkers (CS/PVA–PA–BA hydrogels). In our previous work, anti-drying and thermoplastic CS/PVA/PA hydrogels were successfully prepared and applied as strain sensors, but these sensors lacked adhesion and had moderate sensitivity (GF = 1.77).[31] In this study, through the synergy of PA and BA, CS/PVA–PA–BA hydrogels were capable of adhering to various substrates, including glass, silica rubber, PTFE, steel, and skin, with an ultra-high adhesive strength of 103 kPa on pigskin and 527 kPa on glass. Furthermore, the hydrogel-based strain sensor displays great sensing performance with a wide linear sensing range of up to 1000% (R^2 = 0.996), high sensitivity (GF = 4.61), fast response, and good repeatability. It can be directly attached to human skin for real-time human motion monitoring. Our results point to a feasible strategy for improving the adhesion of hydrogel-based strain sensors through the collaboration of PA and BA and developing high-performance sensing materials with great potential for use in flexible bioelectronics.

2. Results and discussion

2.1. Preparation and characterization of CS/PVA–PA–BA hydrogels

The preparation process of CS/PVA–PA–BA hydrogels is shown in Scheme 1. Solution A with CS, PA, and BA was poured into Solution B with PVA and deionized water to obtain the precursor solution. This solution was then frozen to form CS/PVA–PA–BA hydrogels. As an organic acid, PA generated an acidic environment to dissolve CS. The interaction between PA and PVA/CS was analysed by the FTIR tests (Fig. S1, ESI†).

CS/PVA–PA–10BA hydrogel exhibited a broad band at 3380 cm^{-1}, corresponding to the stretching vibration of O–H groups for PVA and N–H groups for CS. The same band was at a lower wavenumber in the FTIR spectra of PVA (3510 cm^{-1}) and CS (3490 cm^{-1}) and at a higher wavenumber in the FTIR spectrum of CS/PVA–PA–0BA hydrogel (3320 cm^{-1}). The results correspond to the previous study, showing that the phosphate groups of PA could interact with the amine groups of CS by electrostatic interaction and the hydroxyl groups of PVA by hydrogen bonds,[32,33] but the addition of BA slightly hinders these interactions. The freezing step in the hydrogel preparation process caused the partial crystallization of PVA chains. As shown in Fig. S2 (ESI†), the crystallization of PVA was confirmed by the XRD spectrum, where crystalline peaks in the 2θ range of 20–30° and 40° were observed.[34]

Moreover, the ATR-FTIR spectrum of the CS/PVA–PA–10BA hydrogel revealed characteristic peaks at 1411 and 1330 cm^{-1}, corresponding to the B–O stretching from B(OH)$_4^-$ and the BO$_3$ symmetric deformation, respectively (Fig. S3, ESI†).[35] This suggests that a portion of BA ionized into B(OH)$_4^-$. The spectrum also displayed characteristic absorption peaks at 1282 and 662 cm^{-1}. The same peaks were found in the FTIR spectrum of PVA–10BA–HCl hydrogel. According to the literature,[36] these peaks correspond to the stretching vibrations of B–O–C and O–B–O bonds, and the B–O–C bonds are formed by the reaction between hydrolyzed BA (B(OH)$_4^-$) and PVA at a temperature higher than 60 °C and using HCl to generate an acidic condition. CS/PVA–PA–BA hydrogels were also prepared at a high temperature and in an acidic condition generated by PA. Therefore, the network structures of CS/PVA–PA–BA hydrogels were considered to contain covalent B–O–C bridges between B(OH)$_4^-$ and PVA. Overall, CS/PVA–PA–BA hydrogels were crosslinked by multiple interactions, including the hydrogen bonding between PVA and PA, the electrostatic interaction between CS and PA,
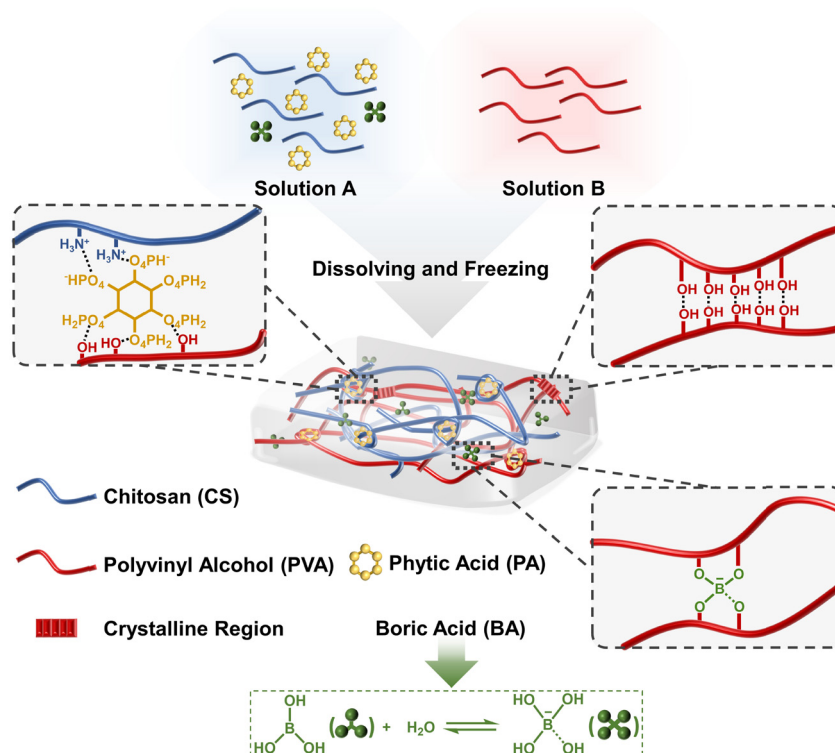
Scheme 1 Schematical illustration of the preparation procedure and the crosslinking structures for CS/PVA–PA–BA hydrogels.

the crystalline regions of PVA, and the B–O–C bonds formed by PVA and $B(OH)_4^-$.

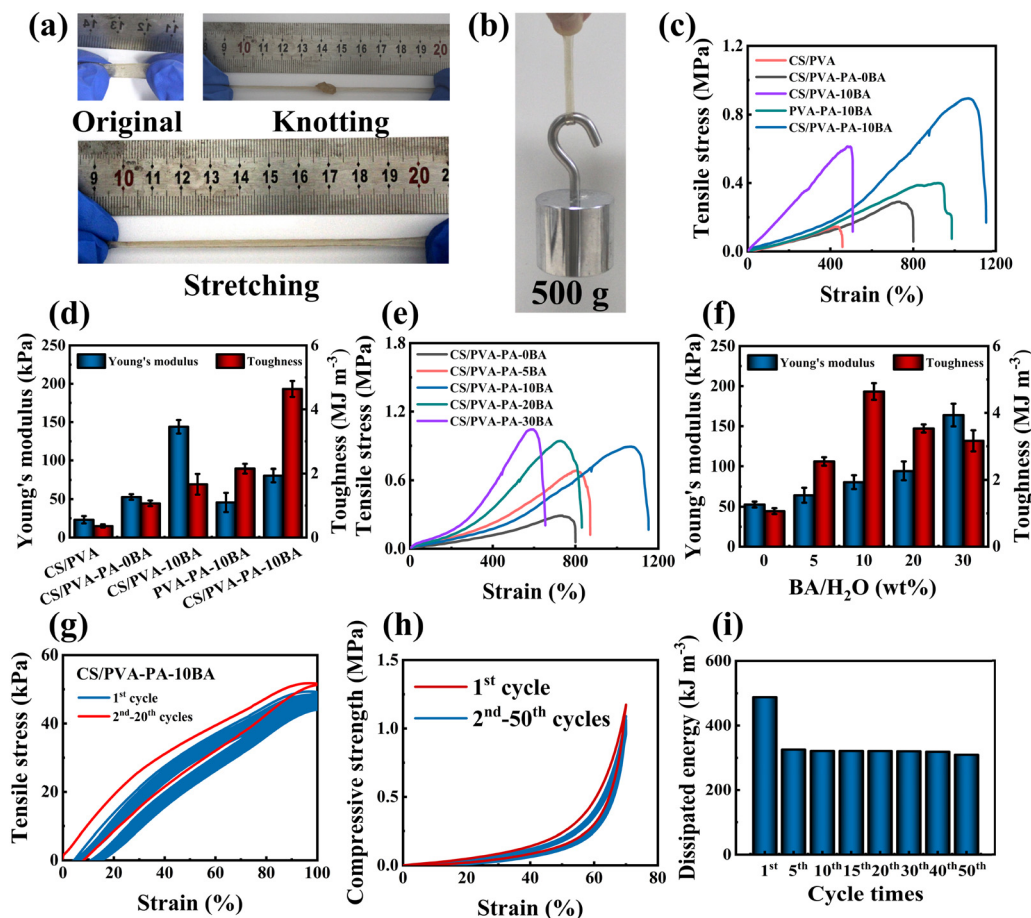## 2.2. Mechanical properties of CS/PVA–PA–BA hydrogels

The CS/PVA–PA–BA hydrogels demonstrated excellent tensile and compression properties. As shown in Fig. 1a and b, these hydrogels could withstand knotting, large stretching deformations, and loadings of 500 g. The mechanical properties of CS/PVA hydrogel were weak but were enhanced by adding PA and BA (Fig. 1c and d). The synergistic effect of PA and BA on mechanical properties was still evident in the absence of CS (PVA–PA–10BA hydrogel). This may be because their addition increased the crosslinking density of the hydrogels. However, although increasing the BA concentrations from 0 to 10 wt%, the fracture strain of CS/PVA–PA–BA hydrogels increased 1.43 times, from $747 \pm 17\%$ to $1070 \pm 50\%$ (Fig. 1e). Further enhancing the BA concentrations to 30 wt%, the fracture strain decreased to $627 \pm 50\%$. Meanwhile, the fracture stress and Young's modulus (Fig. 1f) of CS/PVA–PA–BA hydrogels continuously increased from 0.27 ± 0.01 MPa and 52 ± 3.65 kPa to 1.02 ± 0.05 MPa and 164 ± 14 kPa, and their toughness showed a maximum value at 10 wt% BA concentration (4.64 ± 0.25 MJ m^{-3}). The result indicates that an appropriate amount of BA can enhance the mechanical properties of CS/PVA–PA–BA hydrogels, but the excess amount may limit the movement between the molecular chains due to over-crosslinking, leading to decreased elongation and toughness of CS/PVA–PA–BA hydrogels.[37,38] Successive tensile cyclic stretching-releasing tests were further carried out to estimate

the fatigue resistance of the hydrogels (Fig. 1g). It was found that the hysteresis loop of the hydrogel reduced after the first cycle, but only slightly decreased from the second to twentieth cycles. This implies the good self-recovery of CS/PVA–PA–10BA hydrogel.

The compression properties of CS/PVA–PA–BA hydrogels were also analysed. As shown in Fig. S4 (ESI†), the compressive stress at fracture of CS/PVA–PA–BA hydrogels increased with the increase of BA concentrations from 0 to 30 wt%, and the maximum stress reached 15.65 MPa. Similar to the successive tensile cyclic tests, the cyclic loading–unloading compressive tests of CS/PVA–PA–10BA hydrogel under a 70% strain displayed a reduction of hysteresis loop at the first cycle (Fig. 1h). However, the hysteresis loops overlapped from the 2nd to 50th cycles, and the dissipated energy of the hydrogel was retained at 321.32 kJ m^{-3} after the first cycles (Fig. 1i). The results showed that the hydrogel possessed a good energy dissipation mechanism and excellent self-recovery.

2.3. Adhesion performance of CS/PVA–PA–BA hydrogels

Except for excellent mechanical properties, CS/PVA–PA–BA hydrogels also have great adhesion ability, ensuring a conformable and solid connection with electrodes and the underlying substrates and avoiding the high interface resistance of assisted tapes that leads to motion artifacts. As shown in Fig. 2a, taking CS/PVA–PA–10BA hydrogel as the representative, CS/PVA–PA–BA hydrogels were capable of adhering to various substrates, including polytetrafluoroethylene (PTFE), glass, silica rubber, nitrile rubber, steel, and plastic. Furthermore, it

Fig. 1 Mechanical properties of CS/PVA–PA–BA hydrogels. (a) Photographs of CS/PVA–PA–10BA hydrogel demonstrating knotting, stretching, and (b) lifting a 500 g weight. (c) Tensile stress–strain curves of CS/PVA, CS/PVA–PA–0BA, CS/PVA–10BA, PVA–PA–10BA, and CS/PVA–PA–10BA hydrogels. (d) Corresponding Young's modulus and toughness of these hydrogels. (e) Tensile stress–strain curves of CS/PVA–PA–BA hydrogels. (f) Corresponding Young's modulus and toughness of CS/PVA–PA–BA hydrogels. (g) Twenty-cycle cyclic loading–unloading tensile testing of CS/PVA–PA–10BA hydrogel at 100% strain. (h) Cyclic loading–unloading compressive tests and (i) corresponding energy dissipation of CS/PVA–PA–10BA hydrogel at 70% strain for 50 cycles.

had a robust adhesion to human skin, even suffering from finger bending and stretching (Video S1, ESI†). More impressively, the hydrogel-adhered glass slides could carry a weight of 500 g easily without separation (Fig. 2b and Video S2, ESI†).

To quantify the adhesive strength of CS/PVA–PA–BA hydrogels, the lap shear test was performed. In each test, a piece of hydrogel was sandwiched between a pair of substrates, and two ends of the substrates were fixed on the electronic universal testing machine (Fig. S5, ESI†). The assembled test sample was then stretched until separation between the hydrogel and substrates occurred. The adhesive strengths of CS/PVA–PA–10BA, CS/PVA–PA–0BA, CS/PVA–10BA, CS/PVA, PVA–PA, and PVA–PA–10BA hydrogels on glass are shown in Fig. 2c. The result displayed that the hydrogels containing both PA and BA had higher adhesive strength than the other hydrogels, indicating that the cooperation of PA and BA can synergistically enhance adhesion. Their synergy raised the adhesive strength of CS/PVA hydrogel from 46 kPa to 527 kPa. The adhesion curves of CS/PVA–PA–BA hydrogels with various BA concentrations to different substrates are shown in Fig. 2d–h. Regardless

of the attached substrates, the adhesive strength of CS/PVA–PA–BA hydrogels first improved and then declined with the increased BA concentrations. The maximum adhesive strength was exhibited by the hydrogel with 10 wt% BA (CS/PVA–PA–10BA hydrogel). For example, the adhesive strength of CS/PVA–PA–10BA hydrogel on glass (527 kPa) was 1.68 times higher than that of CS/PVA–PA–0BA hydrogel on glass. In addition, the adhesive strengths of CS/PVA–PA–10BA hydrogel on silica rubber, steel, PTFE, and pigskin were 429, 321, 224, and 103 kPa, respectively.

It is known that both interfacial adhesion and cohesion contribute to the adhesive strength of a hydrogel. Interfacial adhesion is related to the interfacial linkages between a hydrogel and an attached substrate, and it is the basis for the adhesive capability of the hydrogel. Cohesion is related to the toughness of a hydrogel, describing the ability of the hydrogel to resist rupture during peeling.[47] PVA–PA hydrogel had good adhesion (Fig. 2c), whereas pure PVA hydrogel and a hydrogel containing PVA and BA (PVA–BA hydrogel) prepared in the lab could not adhere well to substrates for peeling tests. This

indicates PA has a major impact on the interfacial adhesion of CS/PVA–PA–BA hydrogels. The interfacial adhesion of PA may be from the electrostatic interaction and hydrogen bonding between its phosphate groups and the substrates.[25] However, it should be noted that high concentrations of PA are required when using PA alone as the adhesive component.[24] Although BA alone did not provide sufficient interfacial adhesion, it was found to highly affect the adhesion strength of CS/PVA–PA–BA hydrogels. The variation trend of the adhesion strength of the hydrogels with different amounts of BA was consistent with that of their toughness (Fig. 1f), which implies that BA mainly affects the cohesion of CS/PVA–PA–BA hydrogels. 90° peeling tests of CS/PVA–PA–10BA hydrogel and CS/PVA–PA–0BA hydrogel on glass provided further evidence that BA can cooperate with PA to improve the adhesion of the hydrogels (Fig. 3a).

The adhesion of hydrogels to skin is especially crucial for the application of hydrogels in bioelectronics. A comparison is shown in Fig. 3b between the adhesive strength of CS/PVA–PA–10BA hydrogel and other adhesives (some commercially available adhesives[43–46] and recently reported hydrogel-based adhesives[39–42]) on pigskin. The results display that the adhesive strength of the CS/PVA–PA–10BA hydrogel on pigskin is at least

2.14 times greater than that of the recently reported hydrogel-based adhesives and surpasses that of the commonly used adhesives. Moreover, the hydrogel had stable and repeatable adhesion due to the reversible interactions between it and the substrates. A ten-cycle peeling test of the hydrogel on various substrates was conducted, and at least 63.77% of the adhesion strength was retained after the peeling cycles (Fig. 3c). It is also found that the repeated adhesion performance of CS/PVA–PA–10BA hydrogel was better than that of CS/PVA–PA–0BA hydrogel, indicating that the existence of BA was good for the reusability of CS/PVA–PA–BA hydrogels on adhesion (Fig. S6–S10, ESI†). Moreover, after adhering the CS/PVA–PA–10BA hydrogel to human skin, no residue was left after peeling off (Fig. S11, ESI†). To further verify the residue of hydrogel on the substrates after adhesion, a piece of CS/PVA–PA–10BA hydrogel was stained with Rhodamine B and adhered to glass. As shown in Fig. 3d, the attached and stained hydrogel sample exhibited obvious red fluorescence under the fluorescence microscope. After removing the hydrogel, no fluorescence was observed, suggesting that the hydrogel was peeling off cleanly without leaving residue. The excellent adhesion performance of CS/PVA–PA–10BA hydrogel qualifies it as a novel
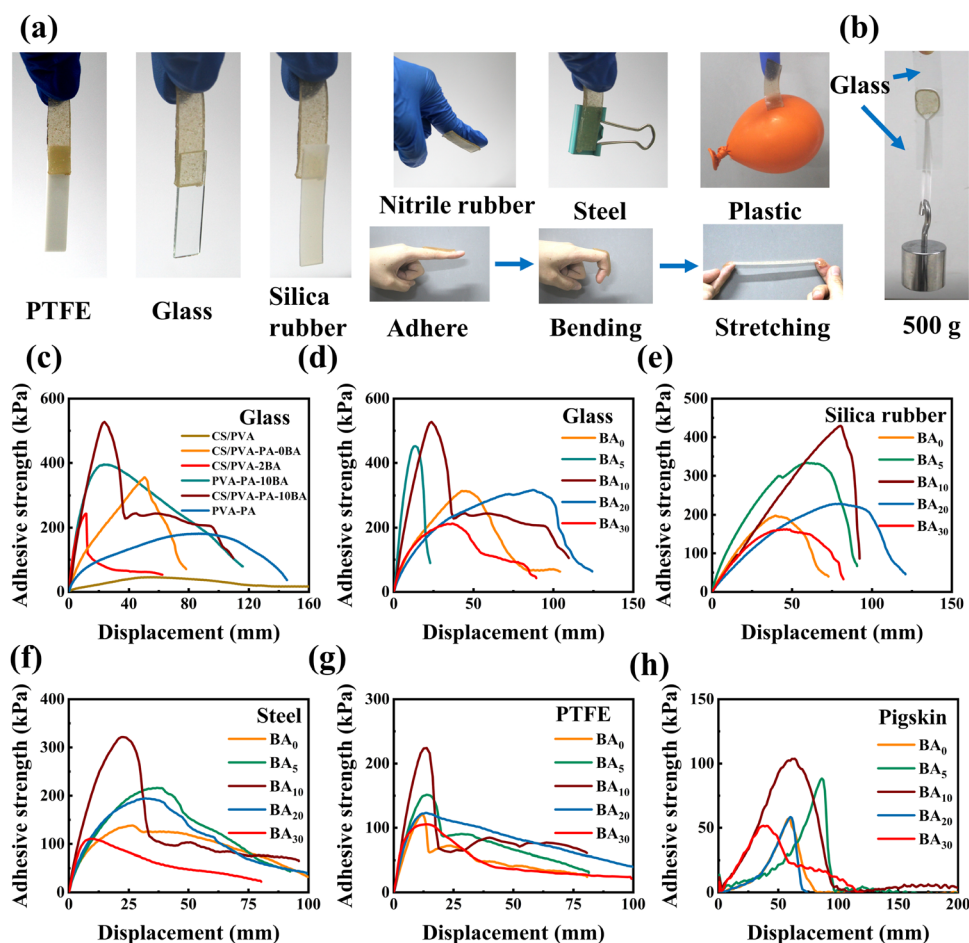

Fig. 2 Adhesive properties of CS/PVA–PA–BA hydrogels. (a) Photographs of CS/PVA–PA–10BA hydrogel adhering to various substrates. (b) The photograph shows that CS/PVA–PA–10BA hydrogel bonding to glass substrates can lift a 500 g weight. (c) Schematic illustration of the lap shear test. Adhesive strength-displacement curves of CS/PVA–PA–BA hydrogels to (d) glass, (e) silica rubber, (f) steel, (g) PTFE, and (h) pigskin.
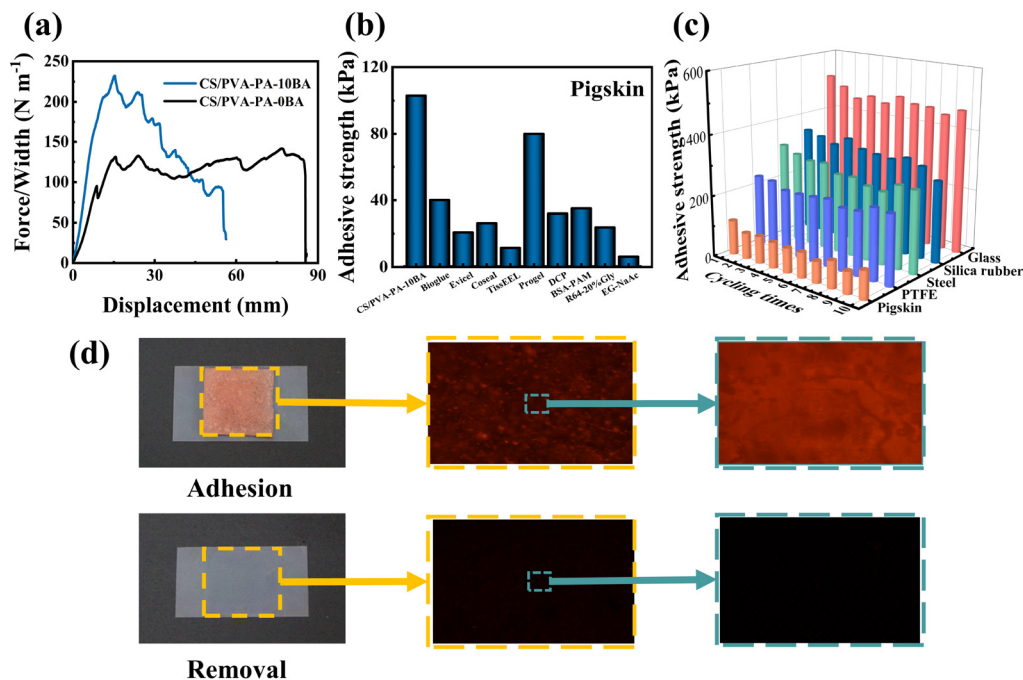
Fig. 3 (a) Adhesion force of CS/PVA–PA–BA hydrogels measured by 90° peeling tests. (b) A comparison of the CS/PVA–PA–10BA hydrogel with recently reported adhesives (PEGSD2/GTU2.5,[39] GT-SA-TPF,[40] Gel-CS,[41] and GFP[42]) and commercially-available adhesives (Bioglue,[43] Evicel, Coseal, Progel,[44] TissEEL,[45] and Cyanoacrylate-based glue[46]). (c) Repeated adhesion of CS/PVA–PA–10BA hydrogel to various substrates. (d) Photographs showing that there is no residue of CS/PVA–PA–10BA hydrogel after peeling off from silica rubber. The hydrogel sample was dyed with rhodamine B.

hydrogel-based adhesive. It is also a good candidate for use in a flexible sensor, which can directly adhere to human skin to monitor physiological activities.

2.4. Sensing performance of the hydrogels

As organic acids, PA and BA produced free hydrogen ions (H^+) after ionization, endowing CS/PVA–PA–BA hydrogels with ionic conductivity. As demonstrated in Fig. 4a, the ionic conductivity of CS/PVA hydrogel was low, and the addition of both PA and BA resulted in increased conductivity. Among all the tested hydrogels, the conductivity of CS/PVA–PA–10BA hydrogel was the highest at 5.3 ± 0.54 S m^{-1}. While the CS/PVA–PA–10BA hydrogel was connected to a simple circuit with a yellow LED, the brightness of the LED gradually dimmed as the hydrogel was stretched from 0 to 700%, indicating that the hydrogel had a resistance response to strain (Fig. 4b). Thus, CS/PVA–PA–10BA hydrogel was assembled into a resistive strain sensor after directly adhering copper electrodes to its two sides.

The strain sensing range, sensitivity, and linearity of the sensor were first estimated. As shown in Fig. 4c, the relative resistance changes of the sensor increased with strain. The sensing range of the sensor was up to 1000% with an excellent linear relationship ($R^2 = 0.996$), which meant the sensor was capable of conveniently outputting precise strain signals. Its GF reached 4.61, suggesting its high sensitivity. Except for its wide linear sensing range and high sensitivity, the sensor also had a fast response and recovery time (Fig. 4d). Upon loading and then unloading to a strain of 50%, the sensor displayed a short

response and recovery times within 90 ms and 140 ms, respectively.

To understand the reason for the high GF and wide linearity of the CS/PVA–PA–10BA hydrogel-based strain sensor, the GF of the sensors based on CS/PVA–PA–10BA, CS/PVA–PA–0BA, CS/PVA–10BA, CS/PVA, and PVA–PA–10BA hydrogels (Fig. S12, ESI†) and the microstructure of these hydrogels before and during stretching (Fig. S13, ESI†) were further studied. It was found that the strain sensors based on hydrogels whose network structure did not show apparent cracks while stretching had linearity. This may be because the breakage of the hydrogel networks leads to the change of their ion transport channels due to blockage, making the resistance of the hydrogel-based strain sensors vary more dramatically,[48] so that these sensors have a surge in GF at large strains, which is unfavorable to linear sensing. Moreover, the sensor based on CS/PVA–PA–10BA hydrogel displayed a higher GF than that based on CS/PVA–PA–0BA hydrogel. The SEM image of these two hydrogels during stretching showed that the network structure of CS/PVA–PA–10BA hydrogel deforms more significantly under stretching than that of CS/PVA–PA–0BA hydrogel. It seemed that higher hydrogel network deformation was beneficial to obtaining a higher GF. In addition, it was found that the GF of the above hydrogel-based sensors increased with the increase of the conductive components (PA and BA) in the hydrogels. The GF of the CS/PVA–PA–30BA hydrogel-based strain sensor was also higher than that of the CS/PVA–PA–10BA hydrogel-based strain sensor (Fig. S14, ESI†), further confirming the increase of conductive components was good for achieving a high GF. This
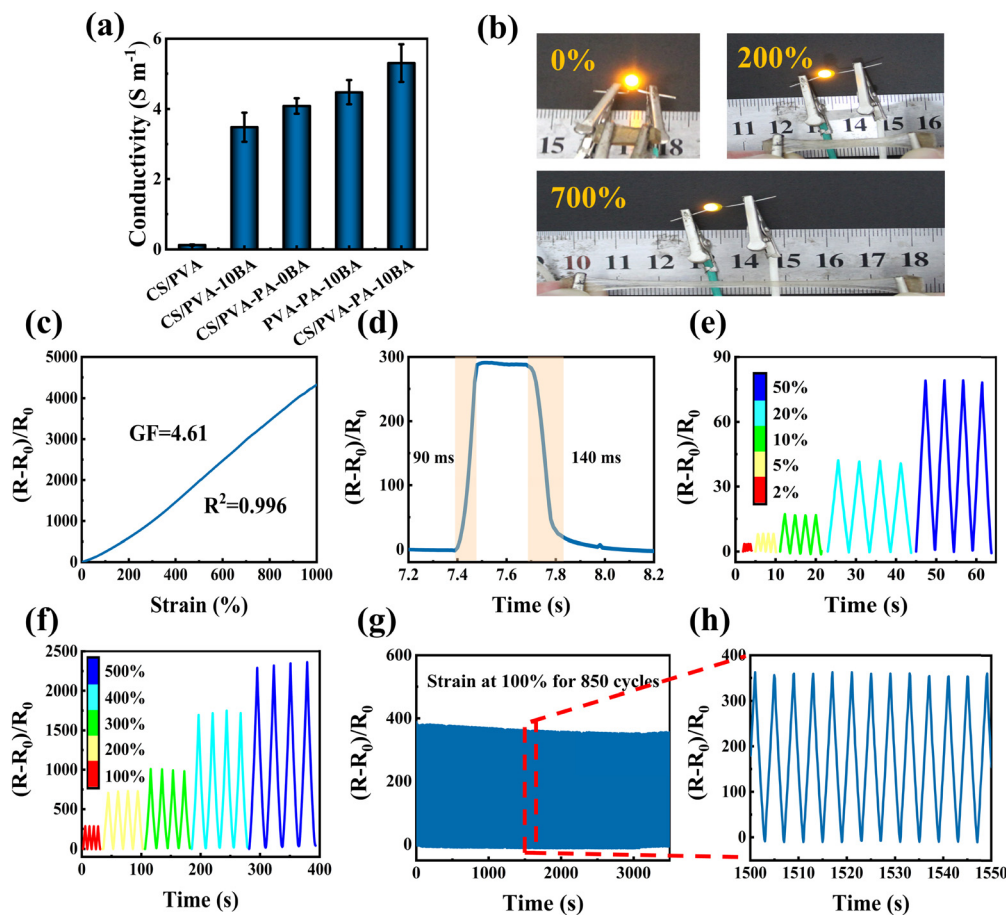
Fig. 4 Strain sensing performance of CS/PVA–PA–10BA hydrogel-based strain sensor. (a) The conductivity of CS/PVA–PA–BA hydrogels. (b) Photographs demonstrating the conductivity changes of the strain sensor by lighting an LED during stretching (0, 200, and 700%). (c) Relative resistance changes and the GF of the strain sensor under various tensile strains (0–1000%). (d) Response and recovery time of the strain sensor under 50% strain. Relative resistance changes of the strain sensor under (e) small strains (2–50%) and (f) large strains (100–500%). (g) Relative resistance changes of the strain sensor under 850 loading–unloading cycles at 100% strain. (h) A zoom-in view of the relative resistance changes from the 364th to 377th loading–unloading cycles.

result may be explained by the fact that the increase in conductive components enables the production of more free ions.[17] Conventional ionic hydrogels usually employ inorganic salts to generate free ions. The "salt-out" effect of the inorganic salts limits their concentrations in the hydrogels. CS/PVA–PA–BA hydrogels use PA and BA to substitute inorganic salts and maintain a stable structure even with large amounts of PA and BA, which benefits the sensitivity of their composed strain sensors.

As shown in Fig. 4e–f, the CS/PVA–PA–10BA hydrogel-based strain sensor maintained good stability and repeatability under both small deformations (2–50%) and large deformations (100–500%). To further explore the durability and stability of the sensor, 850 loading–unloading cycles from 0 to 100% strain were carried out (Fig. 4g). It can be seen that the output signals showed no obvious vibration, and the relative resistance changes of each cycle were basically unchanged (Fig. 4h). The stability of the sensor under different environmental conditions was then studied (Fig. S15, ESI†). The results indicated that the sensing ability of the sensor was maintained well under simulated sweating scenarios, after storage for 30 days, or at 0 °C and 50 °C.

Based on its excellent mechanical properties, self-adhesive ability, and sensing performance, the sensor was used for real-time human motion detection.[49,50] As shown in Fig. 5a, the sensor was directly attached to the finger joint, and its relative resistance changes increased with finger bending from 0° to 90° and dropped once the bending angle was recovered. Similar signal patterns were observed while continuously bending the finger to the same angle. Further adhering the sensor to the wrist and elbow joints, it outputted stable and repeatable signals instantaneously with bending (Fig. 5b and c). In addition, the sensor could distinguish between slow walking and fast running (Fig. 5d and e). It was also sensitive enough to monitor small deformations like speaking and frowning. As shown in Fig. 5f and Fig. S16 (ESI†), the sensor outputted accurate and repeatable signals when it was attached to the throat and the forehead. The results show that the CS/PVA–PA–10BA hydrogel-based strain sensor has good application prospects for human motion monitoring.
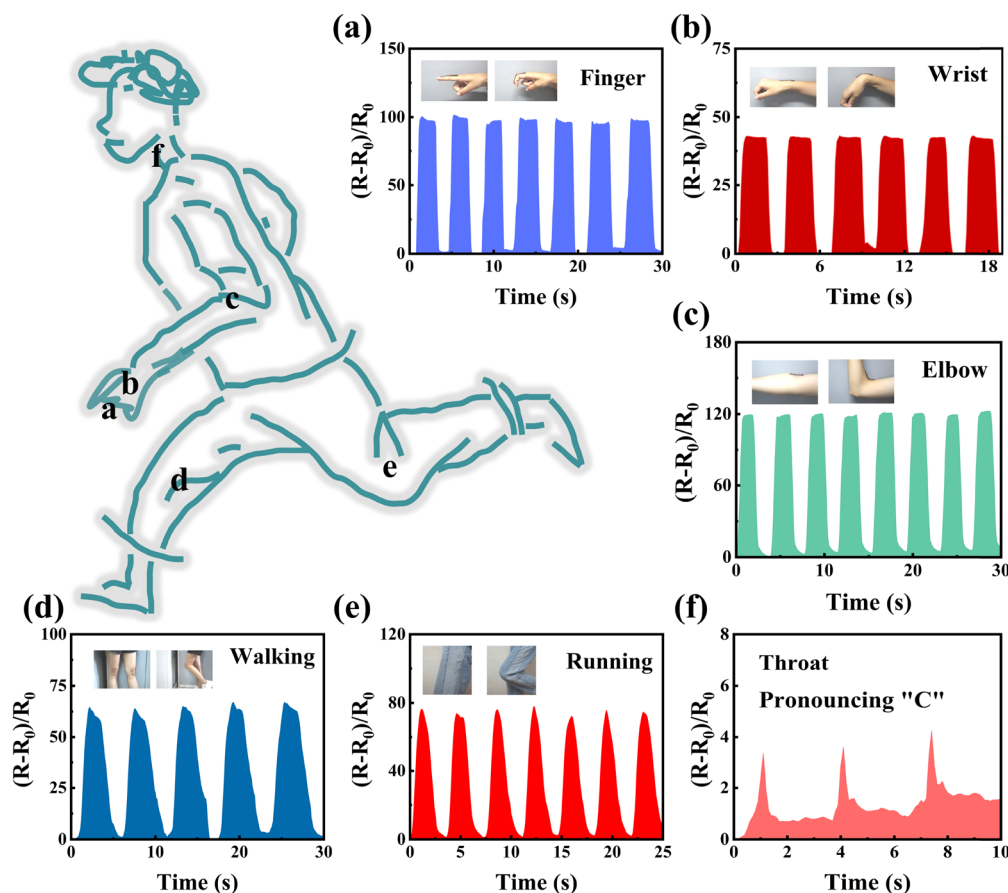
Fig. 5 Real-time monitoring of human activities, including (a) finger bending, (b) wrist bending, (c) elbow bending, (d) walking, (e) running, and (f) speaking, by CS/PVA–PA–10BA hydrogel-based strain sensor.

Fig. S17 and Table S1 (ESI†) show the comparison of the adhesion strength, sensing range, sensitivity, and linearity of this study with the recently reported strain sensors. Compared to other strain sensors,[22,33,51–57] the CS/PVA–PA–10BA hydrogel-based strain sensor has the highest adhesive strength (527 kPa), the widest sensing range (1000%), the highest sensitivity (4.61), and it is linearity. The result demonstrates that the comprehensive performance of the CS/PVA–PA–10BA hydrogel-based strain sensor is at the forefront of the reported strain sensors.

3. Conclusions

In summary, we developed a novel class of tough and highly adhesive CS/PVA–PA–BA hydrogels using a simple mixing method and demonstrated their performance in strain sensors with wide linearity and high sensitivity. The introduction of BA effectively improved the mechanical properties of hydrogels ($1070 \pm 50\%$ of fracture strain, 4.64 ± 0.25 MJ m^{-3} of toughness). Moreover, the hydrogels had outstanding adhesion properties due to the synergy of PA and BA. It was capable of adhering to various substrates, including glass, steel, silica rubber, PTFE, and skin, with a maximum adhesive strength of 527 kPa and a high adhesive strength of 103 kPa on pigskin. The adhesive strength of the hydrogels exceeded many of the commercially available adhesives, such as Bioglue, Evicel, and Progel. Furthermore, the hydrogel-based strain sensor demonstrated high sensitivity (GF = 4.61) and a broad linear sensing range (up to 1000%, R^2 = 0.996) without diverging GF at different strains, in contrast to previously reported strain sensors with a wide strain range. The sensor also exhibited a fast response time (90 ms) and good reproductivity. Based on its excellent sensing performance, the hydrogel-based strain sensor is qualified to accurately and reliably detect human physiological activities by directly attaching to human skin, which has a good prospect in bioelectronics and electronic skins.

4. Experimental section

4.1. Materials

Poly(vinyl alcohol) (PVA, polymerization degree: 1799, molecular weight: 75 kDa) was purchased from Aladdin Biological Technology Co., Ltd. Chitosan (CS) was obtained from Psaitong (degree of deacetylation $\geq$ 85%, viscosity: 200–800 mPa S, molecular weight: 190–310 kDa). Phytic acid (PA, 70% in water) was gained from Adamas. Boric acid (BA) was bought from Guangzhou Haizhu Chemical Reagent Factory. Milli-Q water

(18.2 MΩ cm resistivity at 25 °C) was used in the experiments. All chemicals were used without further purification.

4.2. Preparation of the hydrogels

Firstly, 0.3 g CS and a certain amount of BA were added to a PA solution (4 mL). The mixture was heated and stirred for 1 h at 95 °C to obtain Solution A. Then, Solution B with PVA (1.5 g) and deionized water (1 mL) was added to Solution A, followed by heating and stirring at 95 °C for 1 h. After that, the mixed solution was transferred to a mold and incubated at −15 °C for 24 h to obtain CS/PVA–PA–BA hydrogels. A series of CS/PVA–PA–BA hydrogels have been prepared by the same method. The CS/PVA–PA–BA hydrogels with different amounts of BA were further named CS/PVA–PA–xBA, where "x" represents the mass ratio between BA and deionized water. The other hydrogels are prepared by a similar method with different components: CS/PVA hydrogel is prepared without adding PA and BA; CS/PVA–10BA hydrogel is prepared without PA and with 10 wt% BA; PVA–PA–10BA hydrogel is prepared without CS; PVA–PA hydrogel is prepared with PVA and PA; PVA–10BA–HCl hydrogel is prepared without CS and by adding HCl to adjust the pH to match the hydrogel with PA. The detailed formulas of the hydrogels are listed in Table S2 (ESI†).

4.3. Structure characterizations

The chemical structures of the hydrogels were analysed by their freeze-dried samples using attenuated total reflectance-fourier transform infrared (ATR-FTIR) spectroscopy (Nicolet 170SX FTIR spectrometer) in the wavenumber range of 4000–600 cm^{-1} for 42 consecutive scans at a resolution of 2 cm^{-1}. The microscopic morphology of the hydrogels was studied by scanning electron microscopy (SEM, SIGMA 500, Zeiss) at an acceleration voltage of 15 kV. The hydrogel samples were lyophilized after being frozen by liquid nitrogen directly or under stretching to the maximum sensing range of their correlated strain sensors, and then sprayed with gold under vacuum before observation. The crystalline structures of the hydrogels were tested by X-ray diffractometer (XRD) using a Rigaku Mimi X-ray powder diffractometer (Cu-Kα radiation source) at room temperature in the 2θ range of 5° to 60° with a scanning speed of 5° min^{-1}.

4.4. Mechanical experiments

The tensile and compression tests of the hydrogels were conducted by an electric universal testing machine (Instron 5565) equipped with 500 N load cells at room temperature. The uniaxial and cyclic tensile tests were measured using dumbbell-shaped samples (50 × 4 × 2 mm) at a speed of 50 mm min^{-1}. The Young's modulus was obtained from the slope of the linear region (5–20% strain) from the stress–strain curves. The toughness was calculated from the area below the stress–strain curves. The hydrogel samples, with a diameter of 12 mm and a height of 10 mm, were used for compression tests with a compression speed of 10 mm min^{-1}. Each test was repeated at least three times. The dissipated energy was estimated as the area of the hysteresis loop included in the tensile stretching-releasing curve.[58]

4.5. Adhesion tests

A lap shear test of the hydrogels was conducted using an electronic universal testing machine (Instron 5565) at room temperature. The hydrogels were cut into rectangles of 10 mm in length, 10 mm in width, and 2 mm in thickness. The adhesive surfaces were cleaned with ethanol and deionized water and then thoroughly dried before being bonded by the hydrogels. After adhesion, the peeling samples were pressed with a weight of 50 g for 5 minutes. The adhesion strength of the hydrogels was calculated by dividing the maximal load by the initial attached area. The 90° peeling tests were measured using hydrogel samples with dimensions of 100 (L) × 25 (W) × 2 (T) mm^3. One side of the hydrogel samples was adhered to a piece of glass and pressed with a 700 g weight for 10 minutes. The peeling tests were all performed at a cross-head speed of 5 mm min^{-1}.

4.6. Conductivity measurements

The electrical conductivity of the hydrogels was measured using an electrochemical workstation (PGSTAT302N, Autolab). The FRA impedance potentiostatic mode was selected with a voltage of 10 mV and a frequency range of 10^5–10^{-1} Hz. The hydrogel samples were cut into a strip with a size of 10 mm (length) × 10 mm (width) × 2 mm (thickness). The conductivity (σ) of the hydrogels was calculated by the following equation:

$$\sigma = \frac{L}{RS}$$

where L, R, and S represented the length between adjacent electrodes, the resistance of the hydrogels, and the cross-sectional area of the hydrogels, respectively.

4.7. Strain sensing analysis

To evaluate the performance of CS/PVA–PA–10BA hydrogel as a strain sensor, the hydrogel was cut into strips (50 mm × 5 mm × 2 mm), and then copper strips were attached to both sides of the hydrogel as electrodes. The other hydrogel-based strain sensors are prepared by the same method. Data were collected by a combination of an electronic universal testing machine (Instron 5565) and an LCR meter (TH2829). The response time and recovery time of the hydrogel-based strain sensor were measured by the electrochemical workstation (PGSTAT302N, Autolab). The relative resistance change was defined as $(R − R_0)/R_0 × 100$, where R is the transient resistance and R_0 is the initial resistance. The sensitivity of the sensor was estimated by the gauge factor (GF), which was calculated from the slope of the relative resistance change-strain curve.

Conflicts of interest

There are no conflicts to declare.

Acknowledgements

Notes and references

1 S. Li, P. Cao, F. Li, W. Asghar, Y. Wu, H. Xiao, Y. Liu, Y. Zhou, H. Yang, Y. Zhang, J. Shang, D. Makarov and R. W. Li, *Nano Energy*, 2022, **92**, 106754.

2 X. Di, J. Hou, M. Yang, G. Wu and P. Sun, *Mater. Horiz.*, 2022, **9**, 3057–3069.

3 H. Fu, B. Wang, J. Li, J. Xu, J. Li, J. Zeng, W. Gao and K. Chen, *Mater. Horiz.*, 2022, **9**, 1412–1421.

4 H. Wan, C. Qin and A. Lu, *J. Mater. Chem. A*, 2022, **10**, 17279–17287.

5 A. Zolfagharian, L. Durran, S. Gharaie, B. Rolfe, A. Kaynak and M. Bodaghi, *Sens. Actuators, A*, 2021, **328**, 112774.

6 M. Xie, M. Zhu, Z. Yang, S. Okada and S. Kawamura, *Nano Energy*, 2021, **79**, 105438.

7 R. Yin, D. Wang, S. Zhao, Z. Lou and G. Shen, *Adv. Funct. Mater.*, 2021, **31**, 2008936.

8 M. Zhu, Z. Sun, Z. Zhang, Q. Shi, T. He, H. Liu, T. Chen and C. Lee, *Sci. Adv.*, 2020, **6**, eaaz8693.

9 M. Amjadi, K. U. Kyung, I. Park and M. Sitti, *Adv. Funct. Mater.*, 2016, **26**, 1678–1698.

10 X. Liu, J. Miao, Q. Fan, W. Zhang, X. Zuo, M. Tian, S. Zhu, X. Zhang and L. Qu, *Adv. Fiber Mater.*, 2022, **4**, 361–389.

11 W. Di, Li, K. Ke, J. Jia, J. H. Pu, X. Zhao, R. Y. Bao, Z. Y. Liu, L. Bai, K. Zhang, M. B. Yang and W. Yang, *Small*, 2022, **18**, 2103734.

12 N. Bai, L. Wang, Y. Xue, Y. Wang, X. Hou, G. Li, Y. Zhang, M. Cai, L. Zhao, F. Guan, X. Wei and C. F. Guo, *ACS Nano*, 2022, **16**, 4338–4347.

13 Z. Chen, Y. Chen, M. S. Hedenqvist, C. Chen, C. Cai, H. Li, H. Liu and J. Fu, *J. Mater. Chem. B*, 2021, **9**, 2561–2583.

14 Y. Liu, Q. Liu, L. Zhong, C. C. Chen and Z. Xu, *Chem. Eng. J.*, 2023, **452**, 139314.

15 Y. Guo, X. Wei, S. Gao, W. Yue, Y. Li and G. Shen, *Adv. Funct. Mater.*, 2021, **31**, 2104288.

16 L. Duan, D. R. D'hooge and L. Cardon, *Prog. Mater. Sci.*, 2020, **114**, 100617.

17 G. Li, C. Li, G. Li, D. Yu, Z. Song, H. Wang, X. Liu, H. Liu and W. Liu, *Small*, 2022, **18**, 1–37.

18 Y. Zhao, S. Song, X. Ren, J. Zhang, Q. Lin and Y. Zhao, *Chem. Rev.*, 2022, **122**, 5604–5640.

19 C. Xie, X. Wang, H. He, Y. Ding and X. Lu, *Adv. Funct. Mater.*, 2020, **30**, 1909954.

20 X. Liu, Q. Zhang and G. Gao, *Chem. Eng. J.*, 2020, **394**, 124898.

21 J. Xu, Z. Fan, L. Duan and G. Gao, *Polym. Chem.*, 2018, **9**, 2617–2624.

22 Y. Nie, D. Yue, W. Xiao, W. Wang, H. Chen, L. Bai, L. Yang, H. Yang and D. Wei, *Chem. Eng. J.*, 2022, **436**, 135243.

23 X. Zhang, J. Cao, Y. Yang, X. Wu, Z. Zheng and X. Zhang, *Chem. Eng. J.*, 2019, **374**, 730–737.

24 M. Wang, H. Zhou, H. Du, L. Chen, G. Zhao, H. Liu, X. Jin, W. Chen and A. Ma, *Chem. Eng. J.*, 2022, **446**, 137163.

25 Q. Yu, S. Jin, S. Wang, H. Xiao and Y. Zhao, *Chem. Eng. J.*, 2023, **452**, 139252.

26 X. Zhang, Y. Zhao, S. Wang and X. Jing, *Mater. Chem. Front.*, 2021, **5**, 5534–5548.

27 A. P. Bapat, B. S. Sumerlin and A. Sutti, *Mater. Horiz.*, 2020, **7**, 694–714.

28 S. Cho, S. Y. Hwang, D. X. Oh and J. Park, *J. Mater. Chem. A*, 2021, **9**, 14630–14655.

29 D. Efhamisisi, M. F. Thevenon, Y. Hamzeh, A. N. Karimi, A. Pizzi and K. Pourtahmasi, *ACS Sustainable Chem. Eng.*, 2016, **4**, 2734–2740.

30 X. Li, H. Kang, S. Chen, M. Bai, F. Li, T. Liu, W. Zhou, J. T. Aladejana and J. Li, *J. Cleaner Prod.*, 2023, **397**, 136505.

31 C. Liu, R. Zhang, Y. Wang, Y. Qu, J. Huang, M. Mo, N. Qing and L. Tang, *J. Mater. Chem. A*, 2023, **11**, 2002–2013.

32 L. Xu, C. Wang, Y. Cui, A. Li, Y. Qiao and D. Qiu, *Sci. Adv.*, 2019, **5**, eaau3442.

33 L. Shao, Y. Li, Z. Ma, Y. Bai, J. Wang, P. Zeng, P. Gong, F. Shi, Z. Ji, Y. Qiao, R. Xu, J. Xu, G. Zhang, C. Wang and J. Ma, *ACS Appl. Mater. Interfaces*, 2020, **12**, 26496–26508.

34 Y. Chen, C. Jiao, X. Peng, T. Liu, Y. Shi, M. Liang and H. Wang, *J. Mater. Chem. B*, 2019, **7**, 3243–3249.

35 B. Lu, F. Lin, X. Jiang, J. Cheng, Q. Lu, J. Song, C. Chen and B. Huang, *ACS Sustainable Chem. Eng.*, 2017, **5**, 948–956.

36 K. Park, Y. Oh, P. K. Panda and J. Seo, *Prog. Org. Coat.*, 2022, **173**, 107186.

37 Y. Ye, Y. Zhang, Y. Chen, X. Han and F. Jiang, *Adv. Funct. Mater.*, 2020, **30**, 2003430.

38 X. Yao, S. Zhang, L. Qian, N. Wei, V. Nica, S. Coseri and F. Han, *Adv. Funct. Mater.*, 2022, **32**, 2204565.

39 X. Zhao, Y. Liang, Y. Huang, J. He, Y. Han and B. Guo, *Adv. Funct. Mater.*, 2020, **30**, 1910748.

40 Y. Liang, H. Xu, Z. Li, A. Zhangji and B. Guo, *Nano-Micro Lett.*, 2022, **14**, 1–19.

41 L. Zhou, C. Dai, L. Fan, Y. Jiang, C. Liu, Z. Zhou, P. Guan, Y. Tian, J. Xing, X. Li, Y. Luo, P. Yu, C. Ning and G. Tan, *Adv. Funct. Mater.*, 2021, **31**, 2007457.

42 Y. Yang, K. Shi, K. Yu, F. Xing, H. Lai, Y. Zhou and P. Xiao, *Adv. Healthcare Mater.*, 2022, **11**, 1–9.

43 Y. Hou, X. Zhang, C. Wang and M. Guo, *Processes*, 2020, **8**, 496.

44 N. Annabi, Y.-N. Zhang, A. Assmann, E. S. Sani, G. Cheng, A. D. Lassaletta, A. Vegh, B. Dehghani, G. U. Ruiz-Esparza, X. Wang, S. Gangadharan, A. S. Weiss and A. Khademhosseini, *Sci. Transl. Med.*, 2017, **9**, eaai7466.

45 J. Zhou, A. P. Defante, F. Lin, Y. Xu, J. Yu, Y. Gao, E. Childers, A. Dhinojwala and M. L. Becker, *Biomacromolecules*, 2015, **16**, 266–274.

46 L. Xiao, Y. Sun, Z. Wang, F. Wang, J. Sun, H. Zhang and K. Liu, *Adv. Mater. Technol.*, 2021, **6**, 1–7.

47 H. Montazerian, E. Davoodi, A. Baidya, M. Badv, R. Haghniaz, A. Dalili, A. S. Milani, M. Hoorfar, N. Annabi, A. Khademhosseini and P. S. Weiss, *Chem. Soc. Rev.*, 2022, **51**, 9127–9173.

48 P. Rahmani and A. Shojaei, *Adv. Colloid Interface Sci.*, 2021, **298**, 102553.

49 L. Veeramuthu, C. J. Cho, M. Venkatesan, R. Kumar., G. H. Y. Hsu, B. X. Zhuo, L. J. Kau, M. A. Chung, W. Y. Lee and C. C. Kuo, *Nano Energy*, 2022, **101**, 107592.

50 L. Veeramuthu, C. J. Cho, F. C. Liang, M. Venkatesan, R. Kumar G, H. Y. Hsu, R. J. Chung, C. H. Lee, W. Y. Lee and C. C. Kuo, *ACS Appl. Mater. Interfaces*, 2022, **14**, 30160–30173.

51 F. Lin, Y. Qiu, X. Zheng, Z. Duanmu, Q. Lu, B. Huang, L. Tang and B. Lu, *Chem. Eng. J.*, 2022, **437**, 135286.

52 J. Wen, J. Tang, H. Ning, N. Hu, Y. Zhu, Y. Gong, C. Xu, Q. Zhao, X. Jiang, X. Hu, L. Lei, D. Wu and T. Huang, *Adv. Funct. Mater.*, 2021, **31**, 2011176.

53 D. Wang, J. Zhang, C. Fan, J. Xing, A. Wei, W. Xu, Q. Feng and Q. Wei, *SSRN Electron. J.*, 2022, 110116.

54 A. Wang, Y. Wang, B. Zhang, K. Wan, J. Zhu, J. Xu, C. Zhang and T. Liu, *Chem. Eng. J.*, 2021, **411**, 128506.

55 Y. Yang, Y. Yang, Y. Cao, X. Wang, Y. Chen, H. Liu, Y. Gao, J. Wang, C. Liu, W. Wang, J. K. Yu and D. Wu, *Chem. Eng. J.*, 2021, **403**, 126431.

56 C. Shan, M. Che, A. Cholewinski, J. K. I. Kunihiro, E. K. F. Yim, R. Su and B. Zhao, *Chem. Eng. J.*, 2022, **450**, 138256.

57 X. Sun, Z. Qin, L. Ye, H. Zhang, Q. Yu, X. Wu, J. Li and F. Yao, *Chem. Eng. J.*, 2019, **122832**, 122832.

58 W. Chen, D. Li, Y. Bu, G. Chen, X. Wan and N. Li, *Cellulose*, 2020, **27**, 1113–1126.